Surface & Coatings Technology 206 (2012) 3888–3894

Contents lists available at SciVerse ScienceDirect

Surface & Coatings Technology

journal homepage: www.elsevier.com/locate/surfcoat

# Fabrication of superhydrophobic and oleophobic sol–gel nanocomposite coating

R.V. Lakshmi *, T. Bharathidasan, Parthasarathi Bera, Bharathibai J. Basu *

*Surface Engineering Division, CSIR — National Aerospace Laboratories, Bangalore-560 017, India*

ARTICLE INFO

*Article history:*
Received 25 November 2011
Accepted in revised form 15 March 2012
Available online 23 March 2012

*Keywords:*
Sol–gel
Superhydrophobic
Oleophobic
Nanocomposite
Fluoropolymer
Contact angle

ABSTRACT

Superhydrophobic sol–gel nanocomposite coatings with improved oleophobic property were obtained by incorporation of a perfluoroalkylmethacrylic copolymer in a hybrid sol–gel matrix containing fumed silica nanoparticles. The coatings exhibited a water contact angle (WCA) of 158° and contact angle of 146° for ethylene glycol and 113° for lubricant oil. Though the sol–gel nanocomposite coatings in the absence of fluoropolymer were superhydrophobic with WCA of 155°, they were oleophilic with oil contact angle of <10°. The enhanced oleophobicity can be attributed to the further lowering of surface energy by the presence of fluoropolymer. FESEM images of the coating showed a highly porous structure with random distribution of aggregates of silica nanospheres. The coatings were characterized using FTIR, EDX and XPS. These studies indicated adsorption of fluoropolymer on the coating surface. The method is simple and cost-effective and can be used for preparing multifunctional water- and oil-repellent self-cleaning coatings on large areas of different kinds of substrates like glass, metal and composites.



## 1. Introduction

In the past decade, a large number of different methods has been reported in the literature on the fabrication of superhydrophobic (SH) surfaces with water contact angle (WCA) > 150° and low contact angle hysteresis (CAH) of <5° [1–7]. These surfaces exhibit self-cleaning property and have gained intense interest because of its potential for industrial and practical applications such as anti-fouling paints, micro-fluidics, self-cleaning coatings for architecture, water-proof textiles, etc. It is well known that the superhydrophobicity is governed by both the chemical composition and the geometrical structure of the solid surface. A combination of rough surface having high surface area to volume ratio and low surface energy results in self-cleaning surfaces. However, SH surfaces are generally highly oleophilic. Even though the oleophilic property is made use of for the separation of oil and water, it is not beneficial for several other applications. Therefore, it is important to improve the oleophobicity of SH coatings.

Sol–gel technique has been widely used for the fabrication of SH surfaces due to its inherent advantages like cost-effectiveness, low processing temperature and feasibility of application over large area. Several authors have shown that it is possible to obtain SH surfaces by incorporating nanoparticles and low surface energy materials in sol–gel matrix [8–14]. Superhydrophobic surfaces have also been fabricated by incorporating dual size silica particles in fluoropolymer matrix [15]. However the oleophilic nature of these surfaces causes critical concern for practical applications and hence it is necessary to make them more oleophobic. The surface free energy of the coating can also be lowered by fluorination. It has been reported that oil-repellent SH surfaces can be obtained by modifying the surfaces with fluorochemicals and fluoropolymers resulting in considerable decrease in surface energy [16–22]. The surface energy of functional groups decrease in the order, $-CF_3 < -CF_2H < -CF_2 < -CH_3 < -CH_2$. Perfluoroalkyl methacrylic copolymer has been reported to be useful as fluorinating agents and water repelling additives [20–23].

In the present work, we report a sol–gel nanocomposite coating with binary hierarchical structure which could be prepared by modification of silica nanoparticles with low surface energy perfluoroalkylmethacrylic copolymer (Zonyl 8740) (hereafter referred as FP in the text) via a simple procedure. The formation of the binary microstructure and the hydrophobization with fluoropolymer were achieved simultaneously. The oleophobic SH surface was fabricated on glass and aluminum substrates. The surface morphology was characterized by field emission scanning electron microscopy (FESEM). The surface chemical composition was determined by EDX, FTIR spectra and X-ray photoelectron spectroscopy (XPS) analyses. The wetting property of the coating surface was determined by static and dynamic contact angle measurements. Oleophobicity of the coating was assessed using both ethylene glycol (EG) and lubricant oil with surface tension values 47.7 and 31.0 mN/m respectively.

## 2. Experimental

Methyltriethoxysilane (MTEOS) was purchased from Fluka and ethanol from Merck Chemicals. The perfluoroalkylmethacrylic copolymer (Zonyl 8740, 30% aqueous dispersion) was procured

* Corresponding authors. Tel.: +91 80 25086498.
*E-mail addresses:* lakshmi_rv@nal.res.in (R.V. Lakshmi), bharathi@nal.res.in (B.J. Basu).

0257-8972/$ – see front matter © 2012 Elsevier B.V. All rights reserved.
doi:10.1016/j.surfcoat.2012.03.044

**Table 1**
Contact angles of water, ethylene glycol and lubricant oil of coatings prepared with different precursors and sol mixtures.

| Coating composition | Contact angle (°)[a] | | |
|---|---|---|---|
| | Water | Ethylene glycol | Lubricant oil |
| MT-CS | 89.0 | 69.7 | 46.4 |
| FP | 108.2 | 89.5 | 79.0 |
| MT-CS-FP | 97.3 | 75.7 | 63.6 |
| MT-CS-silica | 155.0 | 43.2 | <10 |
| MT-CS-FP-silica | 158.0 | 146.7 | 113.3 |

[a] Standard deviation, ±2°.

**Table 2**
Static WCA, contact angle hysteresis, sliding angle and average surface roughness values of coatings prepared with different precursors and sol mixtures.

| Coating | Static WCA (°) | CAH (°) | SA (°) | Average surface roughness ($R_a$) (μm) |
|---|---|---|---|---|
| MT | 89.0 | 20–25 | >90 | 0.328 |
| MT | 97.3 | 25–28 | >90 | 1.158 |
| MT | 155.0 | 3–4 | 3 | 2.829 |
| MT | 158.0 | 2–4 | 2 | 2.347 |

from Dupont and was used as received. Colloidal silica (LUDOX® LS, solid contents 30 wt.%, aqueous dispersion) was procured from Sigma Aldrich and fumed silica (Cab-O-Sil type M5 of average particle size 25–30 nm) from M/s Cabot Sanmar Ltd. The preparation of the hybrid sol is described elsewhere [12]. Briefly, the hybrid sol was prepared by mixing equal volumes of MTEOS and colloidal silica and using 1 M acetic acid as the catalyst. The mixture was magnetically stirred for 24 h and then diluted with ethanol. Mixtures of known amounts of hybrid sol and Zonyl 8740 polymer were magnetically stirred for 1 h. Ultrasonically dispersed ethanolic solution of 0.1 g fumed silica was then added to it and further stirred for 1 h. The FP concentration was varied as 0, 1.6, 3.2, 4.8, 6.3, 7.8, 9.2, 11.2 and 13.2 wt.% of the total solid coating. The final mixture of sol, FP and silica dispersion was applied on to the cleaned glass substrate by spraying process. The atomizing air pressure was maintained at 20–25 psi. The coated glass slides were cured at room temperature for 24 h and then heated at 100 °C for 3 h to expel trapped solvents. For comparison, coatings of the hybrid sol as well as that of the FP were prepared on glass substrates by spraying. The thickness of the coatings was in the range of 10–12 μm.

WCA of the coatings were measured by sessile drop method using a Contact angle analyzer, model Phoenix 300 Plus from M/s Surface Electro Optics, South Korea. All measurements made were static contact angles using tangent line-fitting mode. The standard deviation of WCA was found to be ±2°. Sliding angle (SA) measurements were made using a simple instrument fabricated in our laboratory. Both WCA and SA were measured with a drop volume of 8 μL. Deionised Milli Q water (surface tension: 73.2 mN/m) was used for all measurements. Ethylene glycol (EG) and lubricant oil contact angle measurements were also made to determine the oleophobic property of the coatings. An average of five measurements is taken for reporting WCA. The surface morphology of the coatings was studied using FESEM, model Carl Zeiss Supra 40. The scanning electron microscope is equipped with an Energy dispersive X-ray spectrometer (EDX), from Oxford Instruments and was used for the elemental analysis of the coatings. Surface roughness of the coatings was measured by a roughness profilometer from Taylor Hobson (Model Talysurf Intra). The coating thickness was measured using Digimatic micrometer, model Mitutoyo 293–805.

Fourier transform infrared (FTIR) spectra in the absorbance mode were obtained from 20 scans with a Bruker Vector 22 FTIR spectrometer. XPS of sol–gel composite coating was recorded with a spectrometer SPECS, Germany, using non-monochromatic Al Kα radiation (1486.6 eV) run at 13 kV and 300 W as X-ray source. The binding energies ($E_B$) reported here were referenced with C1s peak at 284.5 eV with a precision of ±0.1 eV. For XPS analysis, composite coating was mounted on the sample holder after cutting into small pieces and placed into an ultrahigh vacuum (UHV) chamber at $10^{-9}$ Torr housing the analyzer. All the spectra were obtained with pass energy of 12 eV and step increment of 0.1 eV. Intermittent sputtering was carried out by defocused $Ar^+$ ion beam using QE11/35 ion gun fitted in the preparation chamber of the spectrometer by applying energy of 1 keV at 20 μA beam current with Ar gas pressure of $2\times10^{-5}$ Torr. The experimental data were curve fitted with Gaussian peaks after subtracting a linear background employing PeakFit v4.11 program. The spin-orbit splitting and doublet intensities were fixed as given in the literature [24].

Adhesion of the coating layer with the substrate was assessed according to the ASTM D3359 standard test method using Cross Hatch Cutter, model Elcometer 107. In this test, eleven cuts were made in two directions using the cutter at right angles to each other to form a grid of small squares. A pressure-sensitive adhesive tape was applied over the lattice and removed by pulling in a single smooth action. Adhesion was then assessed by comparing the fraction of coating removed from grid of squares against the ASTM standard ratings. Hardness and scratch resistance of the coating were measured according to the ISO 15184 standard using Pencil Hardness Tester, model Elcometer 501. The pencil hardness test is a constant-load scratch test. It uses pencil leads of different hardness grades (9B–9H) as the scratch stylus. The same normal load with indenters of different

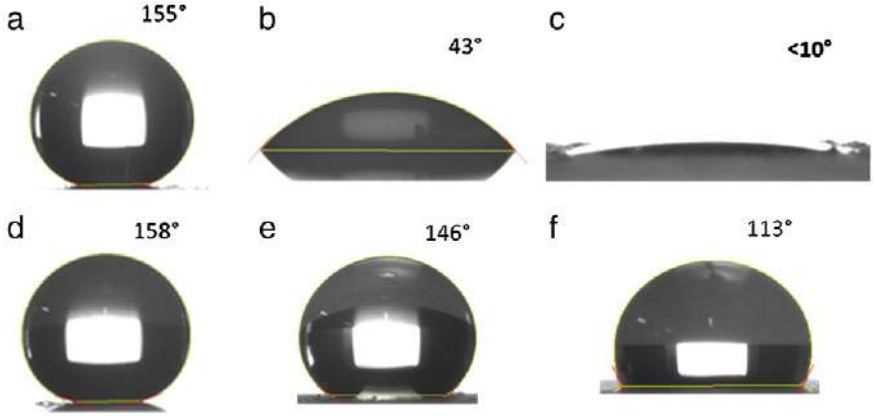


**Fig. 1.** Images of droplets of water (a,d), EG (b,e) and oil (c,f) on MT-CS-silica nanocomposite coatings, without FP (a,b,c), and after incorporating FP (d,e,f).

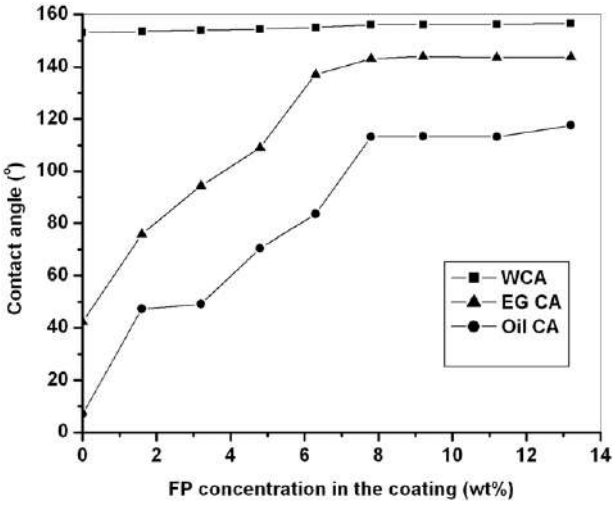


**Fig. 2.** Effect of FP concentration on WCA, EG CA and oil CA of MT-CS-silica nanocomposite coatings.

hardness is applied on the samples. The hardest pencil grade that does not cause damage to the coated specimen is considered as the pencil hardness of the coating.

## 3. Results and discussion

WCA values of sol–gel hybrid coating and the FP coating were 89° and 108° respectively. However, incorporation of FP to the above sol–gel coating showed a decrease in WCA to about 97°. The contact angles of water, EG and lubricant oil of coatings prepared with different precursors and sol mixtures are summarized in Table 1. It can be seen that EG-CA and oil CA of the FP coating also were higher than that of sol–gel coating (MT-CS) and the sol–gel-FP (MT-CS-FP) coatings. After incorporating optimum amount of fumed silica in the sol and sol-FP mixture, the composite coatings obtained exhibited superhydrophobicity with WCA >150°. EG-CA and oil CA of these composite coatings were also determined and included in Table 1. Images of water drop, EG drop and oil drop on sol–gel nanocomposite coatings (MT-CS-silica) with and without FP are shown in Fig. 1. It can be seen that the MT-CS-silica coating (without FP) was superhydrophobic with WCA of 155° whereas the oil CA was <10°. Oil spread on the coating surface quickly and hence the surface was oleophilic. After incorporating FP, the sol–gel-FP-silica coating showed WCA of 158°, EG CA of 146° and oil CA of 113°.

Contact angle hysteresis (CAH) values of the coatings were also measured by a simple method proposed by Callies et al. [25]. The advancing and receding CAs were measured simultaneously by keeping the needle in contact with the drop and moving the substrate by

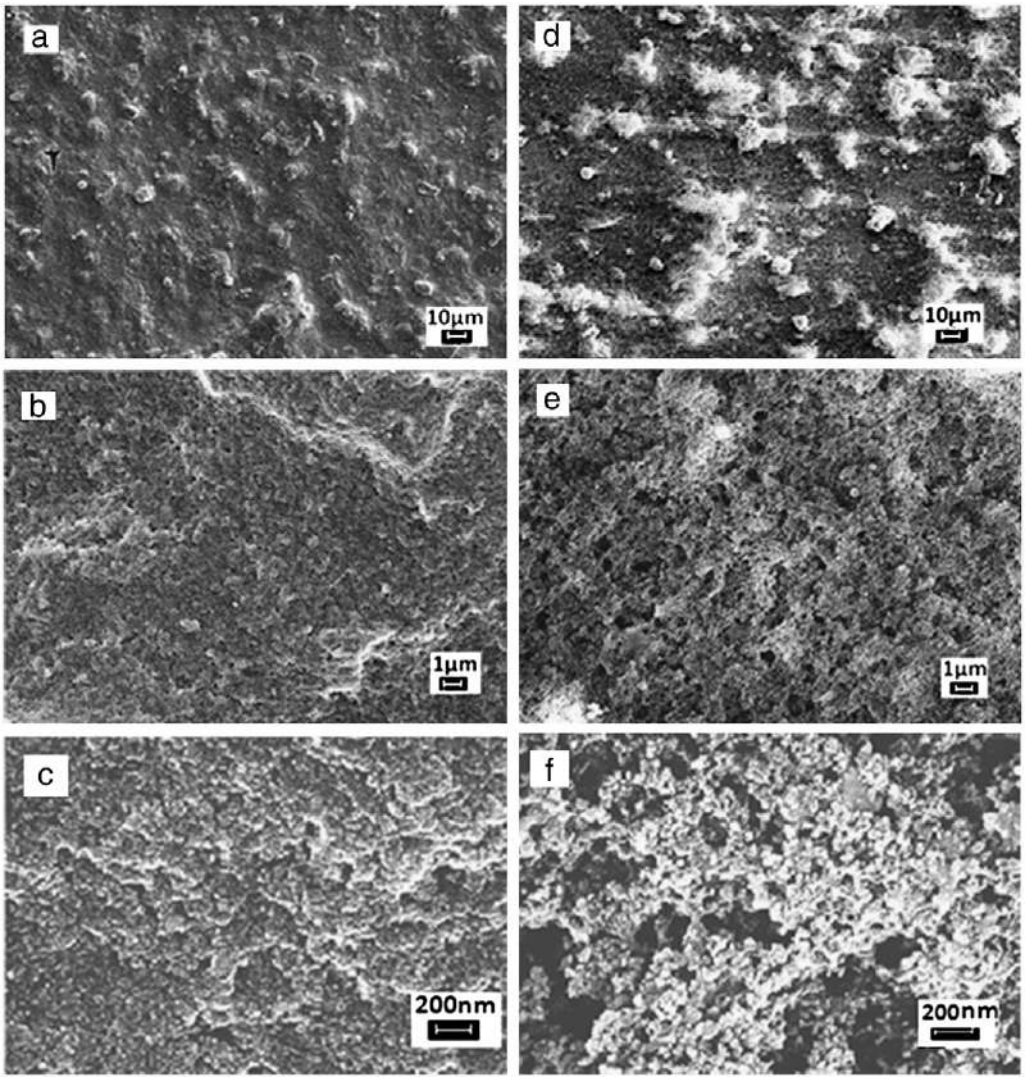


**Fig. 3.** FESEM images of MT-CS-FP coating (a,b,c), and MT-CS-FP-silica coating (d,e,f); magnifications: (a,d) 5.0 KX, (b,e) 25.0 KX and (c,f) 100.0 KX.

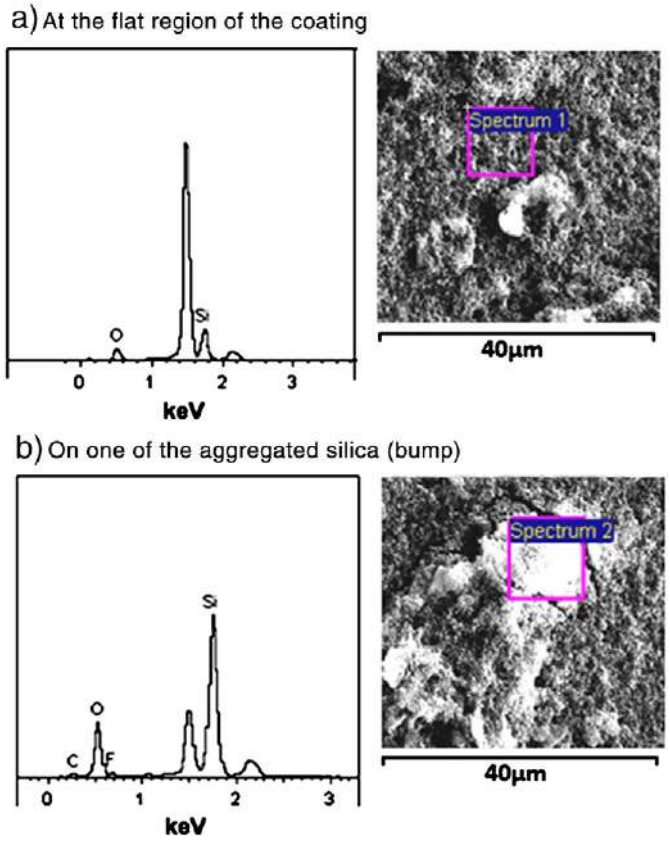


**Fig. 4.** EDX results of the superhydrophobic MT-CS-FP-silica nanocomposite coating.

means of a micrometric screw and CAH was obtained by difference. For comparison, WCA, SA and CAH of the coatings, MT-CS, FP and MT-CS-FP were measured and the results are shown in Table 2. It was found that SAs of these three coatings were >90°. Incorporation of optimum amounts of silica in MT-CS and MT-CS-FP increased WCA and decreased CAH and SA so that the coatings displayed superhydrophobicity and water drops rolled on their surface. It was seen that the CAH values obtained with this method matched with SA values for surfaces with WCA>150° whereas there was no agreement between CAH and SA values for surfaces with WCA<150°. Earlier, Furmidge had shown that surfaces with same hysteresis values do not show the same sliding angles [26]. Their results have shown that direct comparison of sliding angle is preferable to evaluate the sliding properties of surfaces with different contact angles [26,27].

Fig. 2 shows WCA and CAs for EG and lubricant oil of MT-CS-silica coatings prepared with different FP concentrations. WCA of the coatings with different FP concentrations remained 155° and above. Water SA remained <2° for all the coatings. It was found that EG CA and oil CA increased with the increase in FP concentration and reached the maximum value for an optimum FP concentration of 7.8 wt.% of the solid coating. Thus oleophobic property of the coating was significantly enhanced after incorporating the FP. The SA value for EG had reduced from >90° to 20° but oil SA remained >90° at all FP concentrations. This improved oleophobicity can be attributed to the combined effect of low surface energy due to the FP and roughness created by the random distribution of silica aggregates. Further increase in FP did not have any effect on the contact angles of water, EG and oil. Hsieh et al. had observed a slight decrease in EG CA at very high FP concentrations [29]. The FP concentrations used in the present study were comparatively much lower to bring about any decrease in CA. The stability of the water repellency and oil repellency was studied by measuring the WCA, EG CA and oil CA at periodic intervals of 10 min for a duration of 60 min. It was seen that the diameter of the spherical water droplet gradually shrinked with time, whereas the EG drop and oil drop maintained their shapes and the CAs were nearly the same. The oil CA remained the same for more than 24 h indicating excellent stability for oil-repellency.

FESEM images of the MT-CS-FP coatings with and without fumed silica are shown in Fig. 3. Although the MT-CS-FP coating appeared smooth, the image showed evenly distributed micron size bumps (Fig. 3a). FESEM images of MT-CS-FP-silica composite coating clearly showed a highly porous structure with spherical silica particles randomly stacked over the surface. Each silica sphere was about 25–30 nm in diameter and was present in the form of aggregates. These aggregates created a number of peaks and cavities thereby roughening the surface. Such binary structured surfaces easily trap large amount of air within them and make the liquid droplets to rest on a layer of air.

The surface roughness data of the MT-CS-silica coatings with and without FP is shown in Table 2. The average roughness ($R_a$) values of MT-CS-silica and MT-CS-FP-silica composite coatings were 2.829 µm and 2.347 µm respectively. This was much higher compared to the $R_a$ of MT-CS coating which was about 0.328 µm. This increase was mainly due to the distribution of aggregates of fumed silica

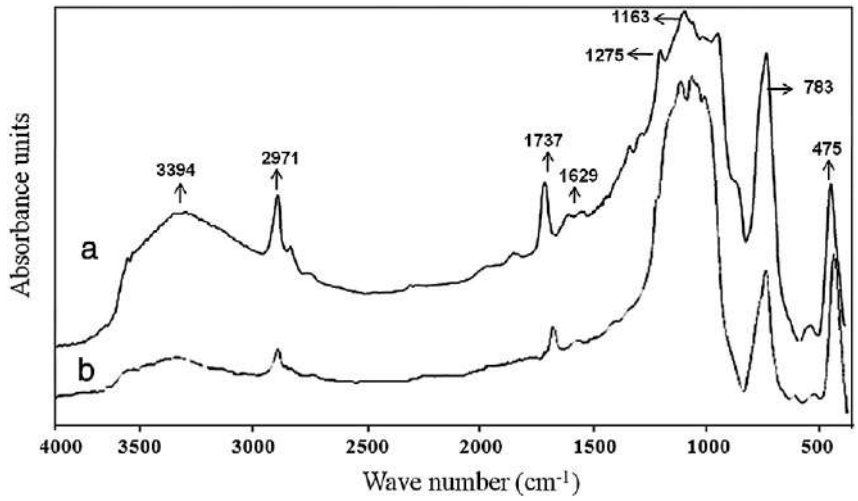


**Fig. 5.** FTIR spectra of (a) MT-CS-FP and (b) MT-CS-FP-silica nanocomposite coatings.

nanoparticles on the coating surface. The composite coatings with different FP concentrations also showed similar $R_a$ values in the range of 2.3–2.5 μm.

The superhydrophobicity of sol–gel composite coatings can be explained using Cassie's model [28]. The apparent CA ($\theta^c$) of a drop on a rough surface is given by Cassie's equation,

$$\cos\theta^c = f_1(\cos\theta_e + 1) - 1 \quad (1)$$

where $f_1$ is the surface area fraction of the solid. As lot of air gets trapped into the valleys between the peaks and protrusions on the rough surface, water drop on such coating only contacts the top of the protrusions resulting in a large water–air interface termed as composite surface which prevents water droplets from penetrating into the valleys and troughs, leading to superhydrophobicity. Miwa et al. have derived an equation describing the relation between WCA and SA on a rough surface [27]. On the basis of their results and calculations, they have shown that a very low SA is attained from a superhydrophobic surface that obeys Cassie's model.

EDX analysis was carried out at different locations on the coating surface — in the flat region and on the bump. The results are shown in Fig. 4 and Table 2. The flat region had fluorine content of 0.7 wt.% whereas fluorine content of 4.7 wt.% was present on the bumps. Thus it is evident that fluorine accumulation was more on the bumps or aggregates compared to the flat region (Fig. 4b). Hence, it can be inferred that FP has more affinity towards silica particles. A similar observation was also made by Hsieh et al. [29]. The Si concentration was found to be nearly the same at both areas. The unlabelled peak in both the cases corresponds to Al, which was used as the substrate. Thus EDX analysis confirmed that FP-adsorbed silica moieties were responsible for the enhanced oleophobicity of the coating. It was seen that F to Si atomic ratio of the coating was about 0.155 and F to Si atomic ratio on the silica aggregate was 0.195. Therefore, very small amount of fluorine was required to render oil repellency to the coating. Hsieh et al. had shown that F to Si atomic ratio of 2 was required to achieve maximum oil repellency for their fluoropolymer composite coatings [29]. Comparatively, the fluorine content was very low for the MT-CS-FP-silica coating described here. This is a major advantage of the present method.

The FTIR spectra for MT-CS-FP and MT-CS-FP-silica composite coatings are shown in Fig. 5. FTIR spectra of the FP and sol–gel-silica coatings were shown in the Supporting information (Figs. S1 and

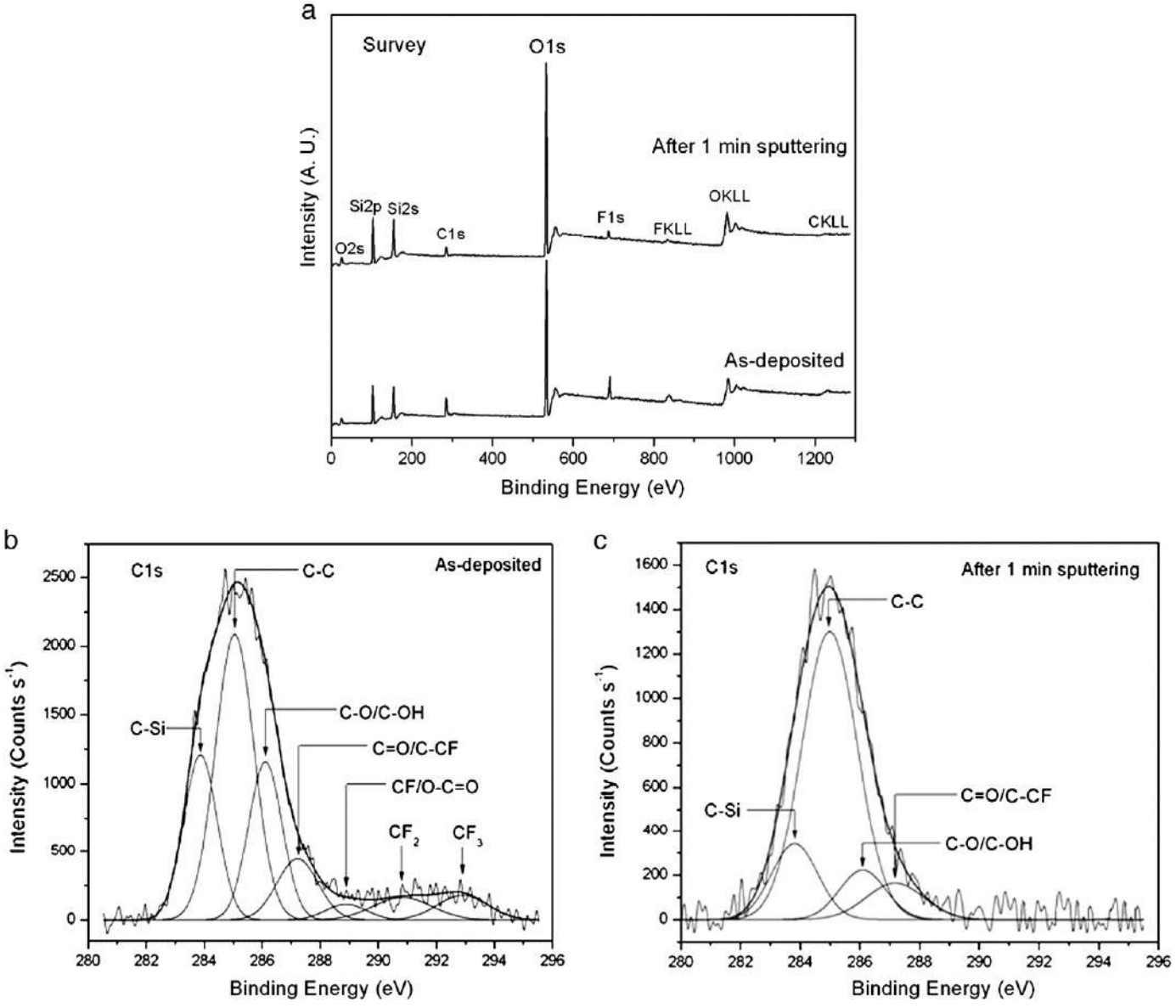


**Fig. 6.** (a) XPS survey spectra of the as-prepared and sputtered MT-CS-FP-silica composite coating; (b) C1s core level spectra of the as-prepared and (c) sputtered coating.

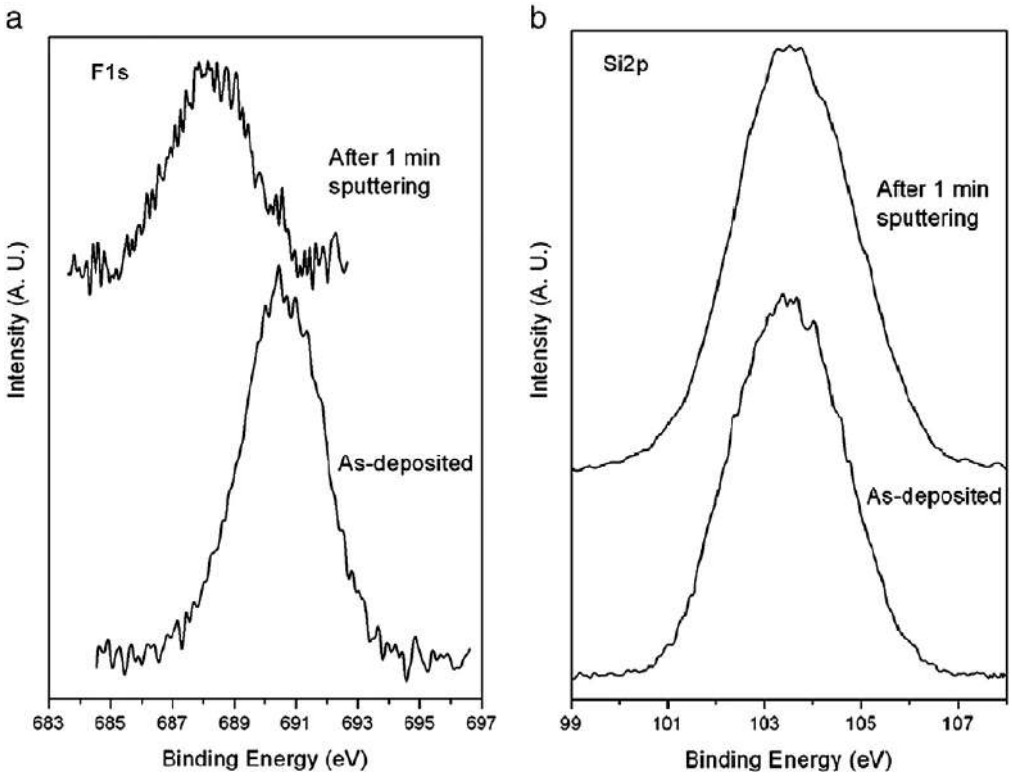


**Fig. 7.** (a) F1s and (b) Si2p core level spectra of the as-prepared and sputtered coating.

S2). The peaks in the FTIR spectrum of MT-CS-FP (Fig. 5a) and MT-CS-FP-silica coating (Fig. 5b) can be assigned as follows. The peaks at 475 and 783 $cm^{-1}$ correspond to the symmetric stretching modes of $SiO_2$ and $Si-CH_3$ group moieties respectively. Strong band due to $Si-O-Si$ moieties is seen at 1000–1163 $cm^{-1}$. The absorbance band at 1375–1275 $cm^{-1}$ corresponds to $CF_3-CF_2-$ group. The peak corresponding to C–F will be at around 1148–1206 $cm^{-1}$ [21,30]. However, it should be noted that the $-Si-O-Si-$ peak in MT-CS-FP-silica coating is slightly broadened and this may be due to the interference of the C–F peak with the siloxane peaks. The strong absorbance band observed at 1737 $cm^{-1}$ corresponds to >C═O of the methacrylate group of the FP. The absorbance band observed at 2971 $cm^{-1}$ corresponds to $-C{=}C-$ stretching mode of the acrylic double bonded carbon atom. A broad peak at 3394 $cm^{-1}$ and small peak at 1629 $cm^{-1}$ corresponds to stretching mode of O–H bonds. Since the FP indicates a peak at 1556 $cm^{-1}$ corresponding to –COOH group [Fig. S1 of Supporting information], the adsorption of FP onto the silica particles may be due to the bonding between –OH group of silica and –COOH group of FP [21].

XPS analysis was carried out to analyze chemical states and composition of elements present in the film surface. Fig. 6(a) shows the survey spectra of MT-CS-FP-silica composite coating before and after sputtering for 1 min. It clearly shows the presence of elements such as C, O, F and Si. There is a decrease in C and F concentrations upon sputtering, whereas concentrations of Si and O get enhanced after sputtering. Individual binding energy region of each element was scanned to get more information about their electronic structure. Spectral envelops of C1s core level of as-deposited and sputtered coating are broad and asymmetrical indicating that several carbon components could be observed in the coating. Deconvoluted spectra of as-prepared and sputtered films are shown in Fig. 6(b, c). Accordingly, peaks at 283.9, 285, 286.1, 287.2, 289.0, 290.8 and 293.0 eV observed in as-prepared film could stand for C–Si, C–C, C–O or C–OH, C═O or C–CF, CF or O–C═O, $CF_2$ and $CF_3$, respectively [31–35]. After 1 min sputtering CF, $CF_2$ and $CF_3$ related peaks disappear. This may be because sputtering must have easily removed the preferentially adsorbed fluorine moieties from the silica surface.

F1s core level spectrum of the MT-CS-FP-silica composite coating is displayed in Fig. 7(a). F1s spectrum of the coating shows a symmetrical peak at 690.4 eV that could be attributed to fluorine moieties with covalent C–F bonds and other $CF_x$ group contributions within C1s spectrum [36]. F1s peak observed at 688.3 eV after 1 min sputtering could be ascribed to $CH_2-CHF$ or CHF–CHF species [34]. Si2p core level spectra of as-deposited and sputtered film are displayed in Fig. 7(b). Si2p core level shows a peak at 103.5 eV and could only be assigned to Si–O species in $SiO_2$ based network [37–39].

**Table 3**
Chemical composition at different regions on the surface of sol–gel-FP-silica composite coatings.

| Element | At the flat region | | On silica aggregate | |
|---|---|---|---|---|
| | Weight % | Atomic % | Weight % | Atomic % |
| C | 18.58 | 26.92 | 11.65 | 17.68 |
| O | 47.90 | 52.10 | 48.02 | 54.70 |
| F | 0.70 | 0.64 | 4.70 | 4.50 |
| Si | 32.83 | 20.34 | 35.64 | 23.12 |

**Table 4**
Pencil hardness of coatings prepared with different precursors and sol mixtures.

| Coating composition | Pencil hardness | Adhesion |
|---|---|---|
| MT-CS sol | >9H | 5B |
| FP | <6B | 5B |
| MT-CS-FP | H | 5B |
| MT-CS-silica | 5H | 5B |
| MT-CS-FP-silica | 2H | 5B |

Relative surface concentrations of F and Si in the MT-CS-silica coatings before and after sputtering have been estimated by the relation [40]:

$$\frac{C_F}{C_{Si}} = \frac{I_F \sigma_{Si} \lambda_{Si} D_{Si}}{I_{Si} \sigma_F \lambda_F D_F}$$

where $C$, $I$, $\sigma$, $\lambda$ and $D$ are the surface concentration, intensity, photoionization cross-section, mean escape depth and analyzer detection efficiency, respectively. Integrated intensities of F1s and Si2p peaks have been taken into account to estimate the concentration, whereas photoionization cross-sections and mean escape depths have been obtained from the literature [41,42]. The geometric factor was taken as 1, because the maximum intensity in this spectrometer is obtained at 90°. Accordingly, relative surface concentration ratios (atomic %) of F/Si in the coating were 0.17 and 0.07 respectively before and after sputtering. Therefore, concentration of F in the coating was found to decrease after sputtering. Thus, XPS analysis confirms that fluorine moieties get desorbed from the surface and the silica framework is exposed on sputtering. This also agrees well with O1s core level spectra shown in Supporting information Fig. S3. The F/Si surface atomic ratio calculated using XPS on as prepared coating is found to agree with that obtained by EDX analysis. This suggests a homogeneous fluorine distribution throughout the overall thickness of the coating. This can be attributed to the presence of silica particles which inhibit the migration and enrichment of fluorine-containing segments towards the surface [43].

The pencil hardness of coatings prepared with different precursor mixtures of sol, FP and silica are summarized in Table 3. The hardness of sol–gel coating was very high whereas that of FP coating was very poor. MT-CS-FP coating had an intermediate hardness value. The hardness ratings of MT-CS-silica, and MT-CS-FP-silica coatings were 5H and 2H respectively (Table 4). Higher hardness of the sol–gel coating is because of the dense siloxane network bonds formed due to the condensation of the silanol groups. Inclusion of FP into the sol might have decreased the integrity of the siloxane network and hence responsible for the reduced hardness. The adhesion with the substrate had the highest rating of 5B for both MT-CS-silica and MT-CS-FP-silica coatings.

## 4. Conclusions

Superhydrophobic and oleophobic sol–gel-silica nanocomposite coatings were prepared by incorporating an optimum amount of commercially available perfluoroalkylmethacrylic copolymer, Zonyl 8740 (FP) in a hybrid sol–gel matrix containing fumed silica nanoparticles. The superhydrophobic sol–gel composite coating was oleophilic, however after incorporating FP, the coating exhibited oleophobic property with ethylene glycol CA of 146° and oil CA of 113°. FESEM images of the coatings revealed its highly porous structure. EDX analysis indicated accumulation of fluorine on silica aggregates. XPS studies also confirmed the preferential adsorption of FP on silica nanoparticles. The improved oleophobicity was attributed to the combined effect of low surface energy due to the FP and roughness created by the random distribution of silica aggregates. Since, the coatings can be prepared on varied substrates, on larger area and complex shapes, it is a facile, cost-effective method to obtain superhydrophobic surfaces with oleophobic property. Another important advantage of the method is that very small amount of fluorine is required to render oil repellency to the coating unlike in other reported methods.

## Acknowledgment

We are grateful to Mr. Shyam Chetty, Director, CSIR-NAL, Bangalore, and Mr. V.K. William Grips, Head, Surface Engineering Division, NAL for their constant support and encouragement for this work. We thank Mr. Siju and Ms. Vanaja for FESEM and FTIR studies respectively. We thank Dr. C. Sudha, IGCAR, Kalpakkam, India for recording XPS of the coating. We greatly appreciate the funding assistance provided by CSIR for carrying out the studies.

## References

[1] X. Zhang, F. Shi, J. Niu, Y. Jiang, Z. Wang, J. Mater. Chem. 18 (2008) 621.
[2] P. Roach, N.J. Shirtcliffe, M.I. Newton, Soft Matter 4 (2008) 224.
[3] X. Li, D. Reinhoudt, M. Crego-Calama, Chem. Soc. Rev. 36 (2007) 1350.
[4] M. Ma, R.M. Hill, Curr. Opin. Colloid Interface Sci. 11 (2006) 193.
[5] X. Deng, L. Mammen, Y. Zhao, P. Lellig, K. Müllen, C. Li, H.J. Butt, D. Vollmer, Adv. Mater. 23 (2011) 2962.
[6] M. Im, H. Im, J.H. Lee, J.B. Yoon, Y.K. Choi, Soft Matter 6 (2010) 1401.
[7] J. Zimmermann, F.A. Reifler, G. Fortunato, L.C. Gerhardt, S. Seeger, Adv. Funct. Mater. 18 (2008) 3662.
[8] C.G. Allen, D.J. Baker, J.M. Albin, H.E. Oertli, D.T. Gillaspie, D.C. Olson, T.E. Furtak, R.T. Collins, Langmuir 24 (2008) 13393.
[9] Q.F. Xu, J.N. Wang, K.D. Sanderson, ACS Nano 4 (2010) 2201.
[10] M. Manca, A. Cannavale, L.D. Marco, A.S. Arico, R. Cingolani, G. Gigli, Langmuir 25 (2009) 6357.
[11] R.V. Lakshmi, B.J. Basu, J. Colloid Interface Sci. 339 (2009) 454.
[12] R.V. Lakshmi, T. Bharathidasan, B.J. Basu, Appl. Surf. Sci. 257 (2011) 10421.
[13] B.J. Basu, V. Hariprakash, S.T. Aruna, R.V. Lakshmi, J. Manasa, B.S. Shruthi, J. Sol–gel Sci. Technol. 56 (2010) 278.
[14] A. Qu, X. Wen, P. Pi, J. Cheng, Z. Yang, Appl. Surf. Sci. 253 (2007) 9430.
[15] A. Qu, X. Wen, P. Pi, J. Cheng, Z. Yang, J. Mater. Sci. Technol. 24 (2008) 693.
[16] P. Fabbri, M. Messori, F. Pilati, R. Taurino, Adv. Polym. Technol. 26 (2007) 182.
[17] H. Wang, J. Fang, T. Cheng, J. Ding, L. Qu, L. Dai, X. Wang, T. Lin, Chem. Commun. (2008) 877.
[18] T. Darmanin, F. Guittard, J. Colloid Interface Sci. 335 (2009) 146.
[19] B. Leng, Z. Shao, G.D. With, W. Ming, Langmuir 25 (2009) 2456.
[20] I.S. Bayer, A. Brown, A. Steele, E. Loth, Appl. Phys. Express 2 (2009) 125003.
[21] H.I. Hsiang, M.T. Liang, H.C. Huang, F.S. Yen, Mater. Res. Bull. 42 (2007) 420.
[22] C.T. Hsieh, J.M. Chen, R.R. Kuo, T.S. Lin, C.-F. Wu, Appl. Surf. Sci. 240 (2005) 318.
[23] S.A. Kulinich, M. Farzaneh, Cold Reg. Sci. Technol. 65 (2011) 60.
[24] D. Briggs, M.P. Seah, Practical Surface Analysis by Auger and X-ray Photoelectron Spectroscopy, Wiley, New York, 1984.
[25] M. Callies, Y. Chen, F. Marty, A. Pe'pin, D. Que're', Microelectron. Eng. 78–79 (2005) 100.
[26] C.G.L. Furmidge, J. Colloid Sci. 17 (1962) 309.
[27] M. Miwa, A. Nakajima, A. Fujishima, K. Hashimoto, T. Watanabe, Langmuir 16 (2000) 5754.
[28] A.B.D. Cassie, S. Baxter, Trans. Faraday Soc. 40 (1944) 546.
[29] C.T. Hsieh, F.L. Wu, W.Y. Chen, Surf. Coat. Technol. 203 (2009) 3377.
[30] J.H. Oh, S.Y. Kwak, S.C. Yang, B.S. Bae, ACS Appl. Mater. Interfaces 2 (2010) 913.
[31] Y.-S. Lee, J. Fluorine Chem. 128 (2007) 392.
[32] H. Liu, R.J. Hamers, Surf. Sci. 416 (1998) 354.
[33] J.Y. Kim, Materials 2 (2009) 1955.
[34] A. Tressaud, E. Durand, C. Labrugère, A.P. Kharitonov, L.N. Kharitonova, J. Fluorine Chem. 128 (2007) 378.
[35] R.W. Jaszewski, H. Schift, B. Schnyder, A. Schneuwly, P. Gröning, Appl. Surf. Sci. 143 (1999) 301.
[36] Y. Ye, Y. Jiang, J. Yu, Z. Wu, H. Zeng, J. Mater. Sci. Mater. Electron. 17 (2006) 1005.
[37] D. Pleul, R. Frenzel, M. Eschner, F. Simon, Anal. Bioanal. Chem. 375 (2003) 1276.
[38] R. Campostrini, M. Ischia, G. Carturan, L. Armelao, J. Sol–gel Sci. Technol. 23 (2002) 107.
[39] L.J. Ward, W.C.E. Schofield, J.P.S. Badyal, A.J. Goodwin, P.J. Merlin, Langmuir 19 (2003) 2110.
[40] C.J. Powell, P.E. Larson, Appl. Surf. Sci. 1 (1978) 186.
[41] J.H. Scofield, J. Electron Spectrosc. Relat. Phenom. 8 (1976) 129.
[42] D.R. Penn, J. Electron Spectrosc. Relat. Phenom. 9 (1976) 29.
[43] Z. Yu, Z. Zhang, Q. Yuan, S. Ying, Adv. Polym. Technol. 21 (2002) 268.